A study of the Relationship Between the Microwave and Meter-Wavelength Emissions from the Solar Flare on June 3, 2021

Julia N. Shamsutdinova,[a,*] **Jinge Zhang,**[b] **Dmitriy A. Zhdanov,**[a] **Larisa K. Kashapova**[a] **and Hamish Reid**[b]

[a]*Institute of Solar-Terrestrial Physics SB RAS,*
Lermontov St. 126A, Irkutsk, Russia

[b]*University College London,*
Gower St, London WC1E 6 BT, United Kingdom

E-mail: yulia@iszf.irk.ru, jinge.zhang.18@ucl.ac.uk, zhdanov@iszf.irk.ru,
lkk@iszf.irk.ru, hamish.reid@ucl.ac.uk

We present a preliminary analysis of a flare event that took place on 3 June 2021 at 01:36 UT. It was observed in microwaves by the Siberian Radioheliograph (SRH) within 3–6 GHz and by the Broadband Microwave Spectropolarimeter (BBMS), and in the meter-wavelength range by the e-Callisto spectrometer network. We found several type III bursts and a type-J burst in the meter-wavelength range. At the same time, only one burst was detected in the averaged time profiles of microwave emission. This one corresponds to the strongest type III radio burst. Using images from the SRH, we defined two sources and separately analysed their time profiles. This approach allowed us to find microwave bursts associated with radio bursts, which were indistinguishable in the averaged time profiles. The observed delays between the microwave and meter-wavelength emissions were compared with the results of a preliminary analysis of dynamic spectra in the meter-wavelength range.

---

*Speaker

1. Introduction

Solar flares are the most powerful phenomena in the Solar system: in tens of minutes, energy release can reaches over 10^{32} ergs. They occur as a result of a fast release of energy previously stored as induced magnetic fields generated by the electric current in the magnetic structures of active regions. Their emission covers a wide range of the electromagnetic spectrum from radio to gamma rays and is also closely related to coronal mass ejections and particle acceleration in the interplanetary space. We usually assume that a flare is a complex of events and the electromagnetic emission corresponding to them (see, for example, [2]).

The traditional scenario of a solar flare includes particle acceleration, plasma heating, and cooling of plasma during the decay phase. The most popular model describing processes during the flare is the so called standard model. According to this model, particle acceleration during the flare occurs high in the corona, then the particles (electrons and ions) with high energies start to move in the contrary directions along magnetic field lines. One group of particles moves downwards to lower layers of the solar atmosphere and generates microwave, X-ray, and chromospheric line emissions. The other part moves up to the corona and further to the interplanetary (IP) space, where they are detected as solar energetic particles (SEP), and accelerated electrons become a source of type III radio bursts (see for details [7]).

The mechanisms of accelerated electron emission at different levels of the solar atmosphere are different. The emission of accelerated electrons happened to be out in the lower levels of the solar atmosphere is usually formed by the incoherent mechanism. The electrons emitting at levels with low density (solar corona and IP space) in the meter-wavelength range do it using the coherent plasma mechanism. However, using the standard model we can expect that if accelerated electrons have a common source, then the microwave and meter-wavelength emission time profiles should show some agreement.

Observations show that the relationship between the microwave and meter-wavelength emissions is complicated. There is no unambiguous answer whether this is due to the insufficient sensitivity of the equipment in the microwave range or is related to the properties of the emission generation by the coherent plasma mechanism. The present study is devoted to the analysis of a weak and short flare allowing us to test the solar flare standard model.

2. Data and analysis

The studied event occurred on June 3, 2021, in active region (AR) 12829 (S18E35). The peak maximum was at 01:36 UT, and the duration of the event was less than a minute. The solar flare had the B1 GOES class. Despite a weak GOES class, this event had a response in a wide range of the electromagnetic spectrum, detected by different instruments.

First, it was observed within the 3-6 GHz range by the Siberian Radioheliograph (SRH) [3]. The Siberian Radioheliograph has a T-shape with a 256-channel antenna, which is used to record microwave emission of solar phenomena within the 3–24 GHz range. The instrument is located at the Radio Astrophysical Observatory (RAO) (Badary urochishche, Buryat Republic). It provides multi-frequency images of the full solar disk with a 1-second resolution. The event was confirmed within 4-8 GHz by the Broadband Microwave Spectropolarimeter (BBMS) operating at the same
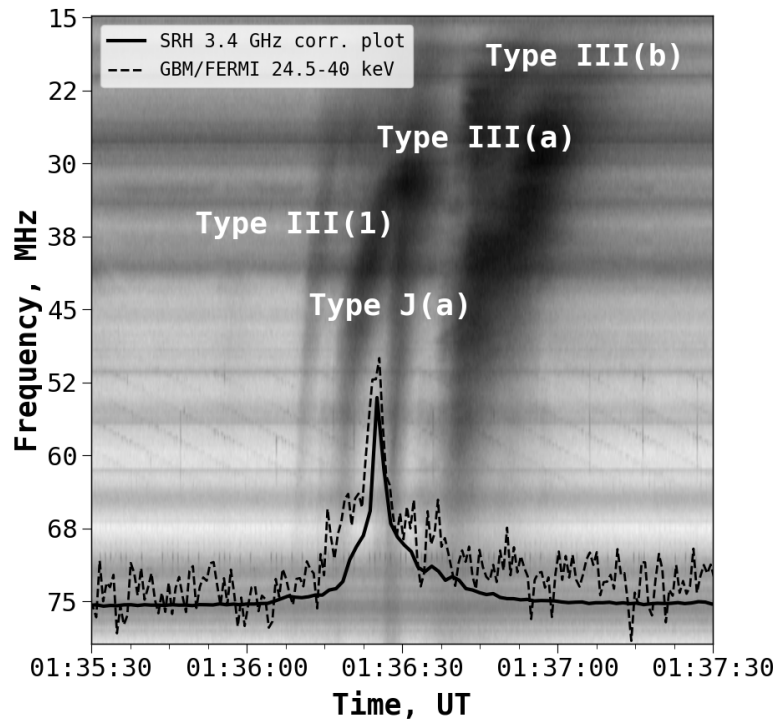
2

Figure 1: The dynamic radio spectrum from e-Callisto (INDIA-GAURI) during the flare SOL2012-06-03T01:35:30. The microwave correlation flux observed by the SRH at a frequency of 3.4 GHz is shown by the solid line. The non-thermal X-ray flux from Fermi/GBM is the dashed line.

observatory [9]. The temporal resolution of BBMS is 1 second. The information about emission in the 15–87 MHz (meter-wavelength) range we obtained from the observations of the e-Callisto spectrometer network [1], GAURI station (India), and ASSA station (Australia). The event also had detectable flux in X-rays as can be seen on the time profiles obtained by the Gamma-Ray Burst Monitor (hereinafter Fermi/GBM) of the Fermi Gamma-Ray Space Telescope [5]. The X-ray emission from Fermi/GBM shows a pronounced response in the energy band above 25 keV that is usually associated with accelerated non-thermal electrons.

Figure 1 shows the dynamic spectrum in the meter-wavelength range overplotted by the X-ray and microwave time profiles. The evolution of microwave emission is shown by the time profile of the correlation coefficients (the correlation graphs) of the SRH at 3.4 GHz [4]. The X-ray evolution is presented by the 25–40 keV flux from Fermi/GBM. We can see only one burst both in the microwave and X-ray ranges. This weak solar flare, on the one hand, judging by the temporal profiles, evolved by a simple scenario, but had a response in a wide range of the electromagnetic spectrum, including non-thermal X-ray emission. Thus, we can conclude that a significant number of accelerated electrons were produced during the flare and the event followed the main rules of the solar flare standard model. But there were at least three bursts in the meter-wavelength range, and the dynamic spectrum looks more complicated. In the dynamic spectrum we see three type III
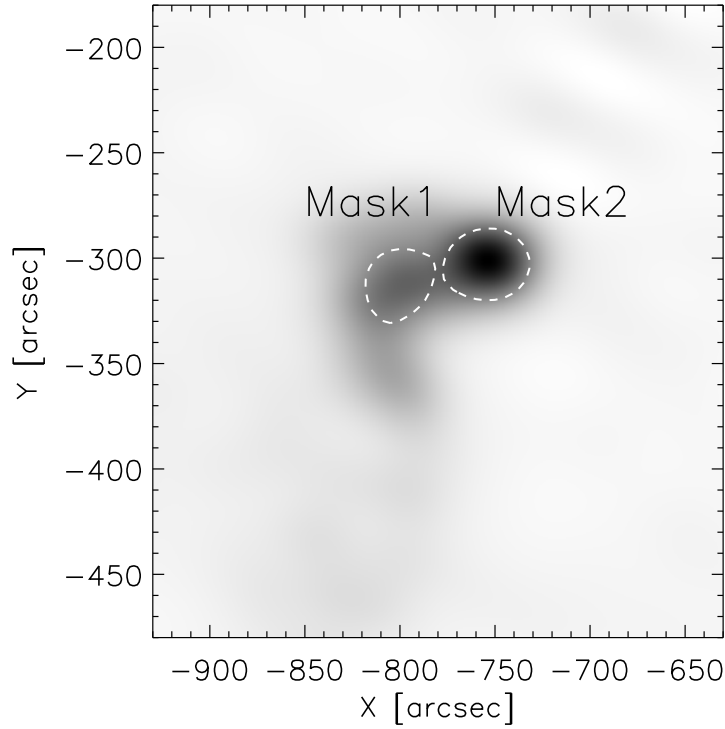
Figure 2: The 3.4 GHz SRH image at 01:36:19 UT. The dashed line contours show the location of two masks.

radio bursts and one type J burst in the meter-wavelength spectrum during the event. The type J bursts are also associated with the motion of accelerated electron beams. In this phenomenon, we see how electrons reach the top of the magnetic loop and after this stop emitting (for more detailed description, see [6]). The questions are if we could find the spatial and physical relationship between the bursts in the meter-wavelength and microwave ranges as well as could we explain the event using the standard model.

Comparison of the time profiles of the X-ray and 75–79 MHz (meter-wavelength) emissions revealed a 15-second delay with an error bar of 1.3 seconds for the most powerful type III burst (b). The error bar is defined by the temporal resolution of the SHR observations. The comparison with the average time profiles of the microwave emission showed the same delay. According to the standard model of the solar flare, the microwave and X-ray emissions generate closer to the initial energy release location, and the delay between these two kinds should be less than 1 second. The delay between the X-ray or microwave emissions and the meter-wavelength emission reflects the travel time of accelerated electrons from the place of the primary energy release (which is indicated by the emission in the X-ray range) to the altitude of emission generation in the 75–79 MHz meter-wavelength range. However, the other meter-wavelength radio bursts are still not associated with bursts in microwaves.

Figure 2 shows the 3.4 GHz SRH image. One can see that the microwave source has a complicated structure and could be presented as a composition of two sources. So, the flare
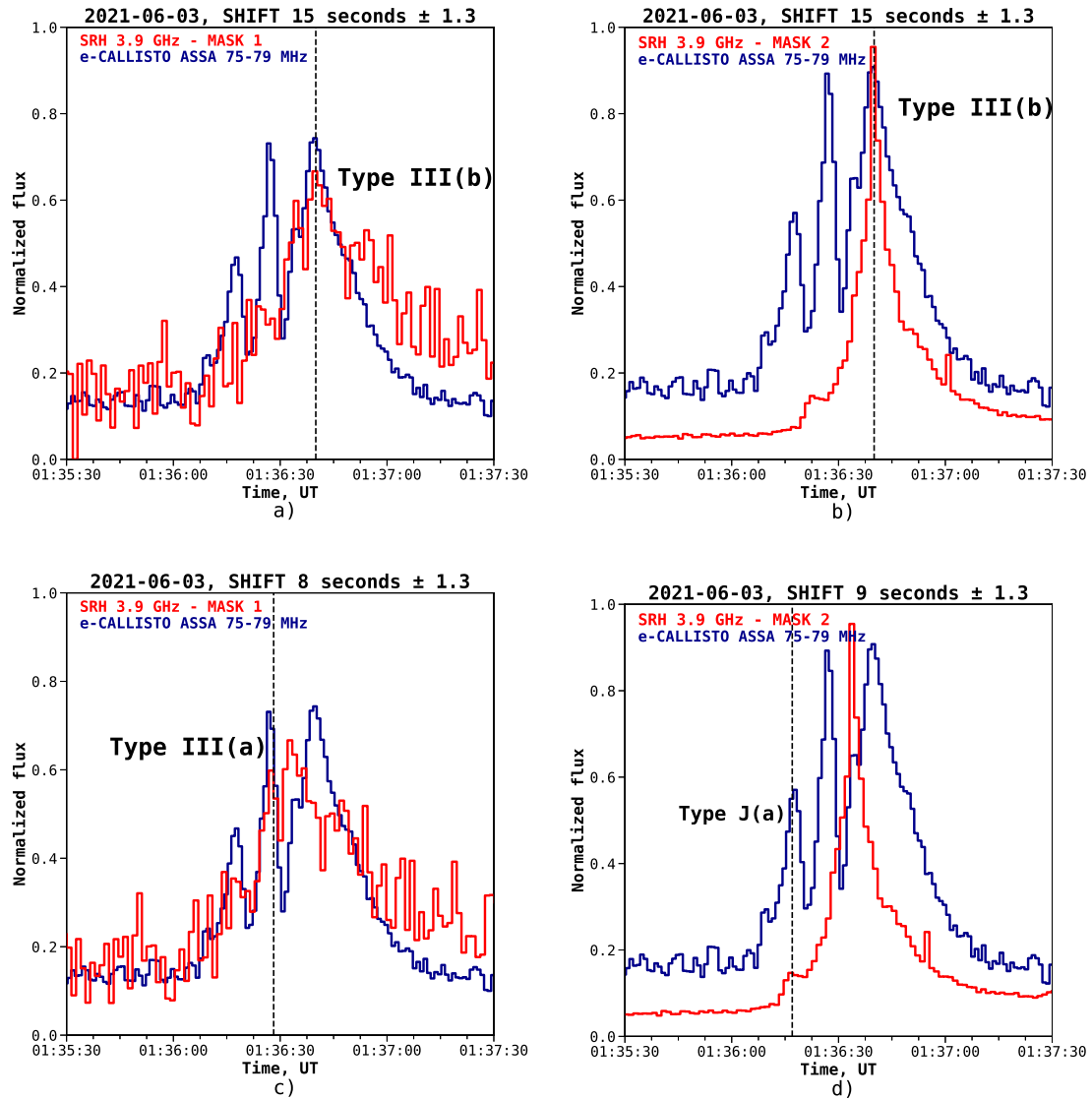
4

Figure 3: Superposition of the e-Callisto (ASSA) average time profile and the time profile taken from the SRH image using masks for the different radio bursts: a) mask 1 for the type III burst (b); b) mask 2 for the type III burst (b); c) mask 1 for the type III burst (a); d) mask 2 for the type J burst (a).

microwave source in the images obtained by the SRH can be divided into two parts using two masks to better understand the microwave emission evolution during the flare. We summed up the images when the eastern part of the microwave flare source was most powerful (between 01:36:01 UT and 01:37:05 UT) and obtained mask 1. The area of mask 1 was determined as the position of the pixels with values above 50 percent of the bright temperature maximum value. The image obtained by summing up the images from 01:36:23 to 01:36:27 UT was used for extracting mask 2. The area of mask 2 was determined as the position of the pixels with values above 80 percent of the bright temperature maximum. The areas of both masks are shown in Figure 2.

Thus, we have obtained fluxes emitted by two sources: eastern (mask 1) and western (mask 2).

The time profiles of the type III burst (b) obtained for mask 1 and mask 2 at the 3.9 GHz frequency show the presence of a response in the two sources with a delay of 15 seconds (see panels "a)" and "b)" in Figure 3). This fact agrees with the results obtained with the average flux in X-rays and microwaves. This could indicate that the eastern and western microwave sources are related to a magnetic loop. However, the western source is more powerful, and we associate it with the primary place of the accelerated electrons release.

We found a response for the type III burst (a) on the time profile obtained for mask 1 . The delay between the microwave and radio bursts was 8 seconds (see panel "c)" in Figure 3). Thus, the origin of the type III burst (a) is related to the eastern microwave source. For the type J burst (a), we found the corresponding burst on the time profile obtained for mask 2 with a 9-second delay (see panel "d)" in Figure 3). The type III burst (1) at about 01:35:52.5 UT was weak and started before the analyzed solar flare. We did not see it in the time profiles of both flare sources. As one can see in Figure 1, mask 1 does not cover all the area of the microwave source. A possible explanation is that the source of the microwave burst related to the type III burst (1) was not covered by the mask.

Table 1: The estimates of the time of electron motion from the place of the primary energy release to the height of the meter-wavelength burst generation in the assumption of the second harmonic

The radio burst	Start frequency, MHz	End frequency, MHz	Beam velocity, c	Delay time, seconds
Type J (a)	75	61	0.17	14.89
Type III (a)	75	58	0.28	9.11
Type III (b)	75	58	0.17	15.25

The information about the delays between the microwave and meter-wavelength bursts could also be obtained from the analysis of the dynamic spectra in the meter-wavelength range. First, we estimated exciter velocities and positions from the frequency drift profile on the radio dynamic spectrum by assuming the magnitude of coronal density models and emission mechanisms. Here we used Saito's model [8] multiplied by a factor of 4.5. Under the second harmonic emission assumption, a radio burst at 20 to 50 MHz correlates to 1.17–1.71 solar radii above the photosphere. Using this, we estimated the travel time of the electron beams generating type III bursts from the level of microwave emission formation to the formation level of the radio emission. This value should correspond to the delay time between the observations in the two ranges. The results are presented in the Table 1. The delays obtained for the type III burst (b) show good correlation with the delay estimated from the meter-wavelength dynamic spectrum. The delay for the type III burst (a) agrees with the obtained delay within the time bins of microwave observations. The delay obtained for the type J burst under assumption of the second harmonic is significantly higher than that taken from the comparison of the microwave and meter-wavelength data. It could mean that accelerated electrons reached the place of the type J burst emission generation faster than the model predicts. The most probable explanation is that the type J burst emission formed by the fundamental harmonic, which is related to a lower height. In this case, the delay should be less than presented in Table 1.

3. Discussion and results.

We carried out the analysis of an event which looked simple in the averaged microwave and X-ray time profiles but had a complicated structure in the meter-wavelength dynamic spectrum. The application of two masks to the images obtained by the SRH in the 3–6 GHz range revealed that two radio bursts, previously not associated with the bursts in microwaves, had corresponding peaks in the microwave range. The type III radio burst for which we did not find a corresponding peak in microwaves could be too weak or located outside the mask locations. A preliminary analysis of the meter-wavelength dynamic spectrum confirmed the obtained relationship and revealed that the type III bursts and the type J burst could be a result of plasma emission at different harmonics.

Based on the study carried out, we can conclude the following.

1. During the considered event, the flux separation using masks of two sources did possibly reveal the relationship between the microwave and meter-wavelength emissions that was not seen in the averaged time profiles.

2. A comparative analysis of the microwave time profiles obtained for different sources with the time profile in the meter-wavelength range revealed that the type III radio burst (b) and the type J burst (a) are associated with the western microwave source. The source of the type III radio burst (a) is related to the eastern microwave source.

3. The relationship between the microwave and meter-wavelength bursts is confirmed by the results of the meter-wavelength dynamic spectra analysis.

4. The present study shows that photometry with angular resolution allows us to investigate the relationship between the microwave and meter-wavelength ranges in more detail.

Acknowledgments

References

[1] Benz, Arnold O., Monstein, Christian, Meyer, Hansueli, *Callisto A New Concept for Solar Radio Spectrometers*, *Solar Physics* **226** (2005) 143-151.

[2] Fletcher L., Dennis B.R., Hudson H.S., et al., *An Observational Overview of Solar Flares*, *Space Science Reviews* **159** (2011) 19-106.

[3] Lesovoi S.V., Altyntsev A.T., Kochanov A.A., et al., *Siberian Radioheliograph : first results*, *Solar-Terrestrial Physics* **3** (2017) 3-18.

[4] Lesovoi S.V., Kobets V.S., *Correlation dependences of the Siberian Radioheliograph*, *Solar-Terrestrial Physics* **3** (2017) 19-25.

[5] Meegan, Charles, Lichti, Giselher, Bhat, P. N., et.al., *The Fermi Gamma-ray Burst Monitor*, *The Astrophysical Journal* **702** (2009) 791-804.

[6] Reid, Hamish A. S., Kontar, Eduard P. *Imaging spectroscopy of type U and J solar radio bursts with LOFAR*, *Astronomy & Astrophysics* **606** (2017) 9.

[7] Reid, Hamish Andrew Sinclair, Ratcliffe, Heather, *A review of solar type III radio bursts*, *Research in Astronomy and Astrophysics* **14** (2014) 773-804.

[8] Saito, K., Poland, A. I., Munro, R. H., *A study of the background corona near solar minimum*, *Solar Physics* **55** (1977) 121.

[9] Zhdanov, D.A., Zandanov, V.G., *Observations of Microwave Fine Structures by the Badary Broadband Microwave Spectropolarimeter and the Siberian Solar Radio Telescope*, *Solar Physics* **290** (2015) 287-294.